



UNIVERSITY OF LEEDS

This is a repository copy of *Structural characterization of a novel GPVI-nanobody complex reveals a biologically active domain-swapped GPVI dimer.*

White Rose Research Online URL for this paper:
<https://eprints.whiterose.ac.uk/175486/>

Version: Accepted Version

Article:

Slater, A, Di, Y, Clark, JC et al. (9 more authors) (2021) Structural characterization of a novel GPVI-nanobody complex reveals a biologically active domain-swapped GPVI dimer. *Blood*, 137 (24). pp. 3443-3453. ISSN 0006-4971

<https://doi.org/10.1182/blood.2020009440>

© 2021 by The American Society of Hematology. This is an author produced version of an article published in *Blood*. Uploaded in accordance with the publisher's self-archiving policy.

Reuse

Items deposited in White Rose Research Online are protected by copyright, with all rights reserved unless indicated otherwise. They may be downloaded and/or printed for private study, or other acts as permitted by national copyright laws. The publisher or other rights holders may allow further reproduction and re-use of the full text version. This is indicated by the licence information on the White Rose Research Online record for the item.

Takedown

If you consider content in White Rose Research Online to be in breach of UK law, please notify us by emailing eprints@whiterose.ac.uk including the URL of the record and the reason for the withdrawal request.



eprints@whiterose.ac.uk
<https://eprints.whiterose.ac.uk/>

Structural characterisation of a novel GPVI nanobody-complex reveals a biologically active domain-swapped GPVI dimer.

Alexandre Slater¹, Ying Di¹, Joanne C. Clark^{1,3}, Natalie J. Jooss^{1,2}, Eleyna M. Martin¹, Fawaz Alenazy¹, Mark R. Thomas¹, Robert A. S. Ariëns⁴, Andrew B. Herr⁵, Natalie S. Poulter^{1,3}, Jonas Emsley^{3,6} and Steve P. Watson^{1,3}.

¹Institute of Cardiovascular Sciences, Level 1 IBR, College of Medical and Dental Sciences, University of Birmingham, Edgbaston, Birmingham B15 2TT, UK

²Department of Biochemistry, Cardiovascular Research Institute Maastricht, Maastricht University, Maastricht, The Netherlands³Centre of Membrane Proteins and Receptors (COMPARE), The Universities of Birmingham and Nottingham, The Midlands, UK⁴Discovery and Translational Science Department, Leeds Institute of Cardiovascular and Metabolic Medicine, University of Leeds, UK

⁵Division of Immunobiology and Division of Infectious Diseases, Cincinnati Children's Hospital Medical Center, Cincinnati, OH

⁶School of Pharmacy, Biodiscovery Institute, University Park, University of Nottingham, Nottingham NG7 2RD, UK

Corresponding authors: Alexandre Slater (a.slater@bham.ac.uk), Steve P Watson (S.P.Watson@bham.ac.uk) Institute of Cardiovascular Sciences, IBR Building, College of Medical and Dental Sciences, University of Birmingham, Birmingham B15 2TT, UK.

Abstract word count: 249

Text word count: 3998

Number of Figures 6

Tables: 1

Number of references: 30

Running title: Structure of GPVI-nanobody complex

Scientific category: Thrombosis and Haemostasis

Key points

The binding site of a novel inhibitory nanobody to GPVI has been mapped and shown to lie adjacent to the binding site of CRP.

The structure of GPVI in complex with an inhibitory nanobody reveals a novel domain swapped conformation implicated in platelet signalling.

Abstract

GPVI is the major signalling receptor for collagen on platelets. We have raised 54 nanobodies (Nb), grouped into 33 structural classes based on their complementary determining region 3 (CDR3) loops, against recombinant GPVI-Fc (dimeric GPVI) and have characterised their ability to bind recombinant GPVI, resting and activated platelets, and to inhibit platelet activation by collagen. Nanobodies from six different binding classes showed the strongest binding to recombinant GPVI-Fc suggesting that there was not a single dominant class. The most potent three, Nb2, 21 and 35, inhibited collagen-induced platelet aggregation with nanomolar IC₅₀ values and inhibited platelet aggregation under flow. The binding K_D of the most potent Nb, Nb2, against recombinant monomeric and dimeric GPVI was 0.6 and 0.7 nM, respectively. The crystal structure of monomeric GPVI in complex with Nb2 revealed a binding epitope adjacent to the CRP binding groove within the D1 domain. In addition, a novel conformation of GPVI involving a domain swap between the D2 domains was observed. The domain swap is facilitated by the outward extension of the C-C' loop which forms the domain swap hinge. The functional significance of this conformation was tested by truncating the hinge region so that the domain swap cannot occur. Nb2 was still able to displace collagen and CRP binding to the mutant, but signalling was abolished in a cell-based NFAT-reporter assay. This demonstrates that the C-C' loop region is important for GPVI signalling but not ligand binding and suggests the domain-swapped structure may represent an active GPVI conformation.

Introduction

The platelet glycoprotein VI (GPVI) has been identified as an attractive anti-thrombotic target ¹. GPVI is the major platelet signalling receptor for collagen ², and is a receptor for other ligands, including fibrin ^{3,4}. GPVI consists of two N-terminal immunoglobulin (Ig)-like domains (D1 and D2), a highly O-glycosylated and sialylated stalk region, a single trans-membrane spanning helix and a short intracellular tail ⁵. There is a single N-glycosylation site in the D1 domain. GPVI signalling requires the FcR γ -chain homodimer, which associates through a salt bridge in the trans-membrane region of GPVI ⁶. Ligand binding occurs through the D1 domain ^{7,8} and leads to phosphorylation of the two conserved tyrosines within the immunoreceptor tyrosine based activation motif (ITAM), present on the FcR γ -chain, by Src family kinases ⁹⁻¹¹. Phosphorylation of the ITAM allows the recruitment of the tyrosine kinase Syk via its tandem SH2 domains and further downstream signalling ¹².

GPVI has been proposed to exist as a monomer and dimer in the membrane ¹³⁻¹⁵. The group of Moroi and Jung reported that recombinant dimeric GPVI, where the extracellular domains are fused to the dimeric Fc domain from IgG, but not monomeric GPVI, binds to collagen with micromolar affinity ¹⁶. They proposed that the differential binding was due either to increased avidity or to the formation of a dimer-specific epitope. The latter was supported by the discovery of several dimer-specific antibodies that detected increased expression upon platelet activation ¹³⁻¹⁵. Since GPVI is not present in intracellular stores in platelets, this suggests that the increase in binding is due to a conformational change as a result of dimerisation.

The crystal structure of the recombinant GPVI extracellular domain has been solved for both unbound (PDB: 2GI7 and 5OU7) and collagen-related-peptide (CRP) bound forms (PDB: 5OU8 and 5OU9),

with both structures revealing a back-to-back dimerisation interface present within the D2 domain. Additionally, collagen is able to cluster GPVI receptors on the platelet membrane surface¹⁷ and therefore generate higher order oligomers. GPVI-signalling occurs once a critical level of clustering has been reached. The concept of a dimer-specific epitope in GPVI is not supported by the crystal structure of CRP-bound to GPVI which shows binding in the D1 domain and suggests a 1 : 1 stoichiometry rather than *de novo* formation of a binding epitope. Additionally, the site of binding of the dimer-specific antibodies and the mechanism whereby platelet activation leads to an increase in dimerisation, are required to establish a full understanding of the role of dimerisation in platelet activation by GPVI.

Nanobodies have emerged as potential therapeutic agents which have the same antigen specificity and binding affinity as full length antibodies but are approximately a tenth of the size. The smaller size makes them more suitable to a variety of techniques including fluorescent imaging¹⁸ as well as having greater tissue penetration. Nanobodies are comprised of a single variable domain derived from antibodies produced by camelids, which differ from human antibodies in that they do not have a light chain component and consist of two disulphide-linked heavy chains¹⁹. In this report we have raised and characterised over 50 nanobodies against dimeric GPVI with the aim of producing a series of GPVI conformation-specific reagents. By solving the complex structure of GPVI with Nb2, the most potent GPVI inhibitory nanobody, we have revealed a novel domain swapped GPVI-dimer and mapped its binding site adjacent to that of CRP.

Methods

Materials

Recombinant GPVI-Fc γ (GPVI residues 1-183) was expressed in the SigpIg⁺ plasmid as previously reported²⁰. Nanobodies were raised against GPVI through VIB Nanobody core (VIB Nanobody Service Facility, Brussels, <https://corefacilities.vib.be/nsf>) and the DNA sequences were provided in PMECS vector. Goat anti-human immunoglobulin G (IgG) and rabbit anti-6-His HRP antibodies were purchased from ThermoFisher Scientific (Glasgow, United Kingdom) and Cambridge Bioscience (Cambridge, United Kingdom) respectively. Alexa Fluor-647 rabbit anti-6-His was purchased from ThermoFisher Scientific (Paisley, UK). Collagen was purchased from Nicomed and collagen related peptide (CRP) was prepared as previously described²¹. CRP-XL was purchased from CAMBOL laboratories (Cambridge, UK). CD62P-PE and isotype IgG1 κ -PE were from Biolegend (San Diego, Ca, USA). PAR1 activating peptide (SFLLRN) was purchased from Severn Biotech (Kidderminster, UK)

PCR mutagenesis

Site-directed mutagenesis was performed on GPVI to produce the glycosylation (N72/Q), domain swap hinge deletion mutants and thrombin cleavable nanobodies. All mutagenesis was performed using a Q5 site-directed mutagenesis kit (New England Biolabs) following the provided protocol. The primers used are shown in Supplemental Table 1.

Expression and purification of recombinant GPVI

GPVI-Fc (dimeric) was expressed and purified in the SigpIg expression vector as previously described²⁰. The construct consists of both the D1 and D2 domains (residues 1-183), but does not contain the stalk like other GPVI-Fc constructs including Revacept²². Monomeric GPVI was produced by cleavage of the Fc domain by incubating with human Factor Xa for 12-18 hours at room temperature (1 μ g FXa for every 250 μ g of GPVI) in the presence of 2.5 mM CaCl₂. Protein-A chromatography was used to separate the cleaved Fc and GPVI followed by gel filtration using a Superdex 75 26/60. All proteins were snap frozen and stored at -80 °C.

Expression and purification of GPVI nanobodies.

All nanobodies were expressed in *E.coli* wk6 cells and contain an N-terminal PelB sequence, that allows for secretion of the nanobodies into the periplasmic space, and C-terminal HA and His tags. Nanobodies were purified using nickel affinity chromatography. For crystallography experiments, the tags were removed by thrombin cleavage. Detailed description of the nanobody purification is provided in the Supplemental methods.

Solid-phase binding assay

Solid-phase binding assays were performed following previously documented experimental protocols²⁰. Wells were coated with collagen (4 µg/ml), CRP (4 µg/ml) or GPVI-Fc (1 µg/ml). HRP-conjugated anti-Fc antibody was used for the detection of GPVI-Fc binding and HRP-conjugated anti-His was used for the detection of nanobody binding.

Flow cytometry

Washed platelets (2×10^7 /mL) were incubated with vehicle or PAR1 peptide (200 µM) for 3 min at room temp. Platelets were then incubated with each nanobodies (5 µM) and binding was detected with Alexa Fluor-647 rabbit anti-6-His antibody. Detailed description of the methods is provided in the Supplemental methods.

Platelet aggregation assay

Human platelets were freshly prepared and aggregation measured as previously described²⁰. Platelets were incubated with the nanobody for 10 min before stimulation with 5 µg/ mL collagen or 10 µg/ mL CRP-XL. The effect of different concentrations of the nanobody compared to PBS was determined using two-way ANOVA with Dunnett's correction for multiple comparisons

Whole blood microfluidics

500 µl of whole blood was flown over Horm Collagen I (100 µg/ml) through a Maastricht parallel flow chamber at a shear rate of 1000/s at room temperature as described before²³. Blood was treated with either PBS or nanobody (500 nM). Brightfield and fluorescence images were quantified for surface area coverage by specific semi-automated ImageJ scripts²⁴. Full methods are reported in the Supplemental methods.

Surface plasmon resonance

Surface plasmon resonance experiments were performed using a Biacore T200 instrument (GE Healthcare). GPVI was immobilised directly onto the CM5 chip using amine-coupling. Reference surfaces were blocked using 1M ethanolamine pH 8. All sensograms shown are double reference subtracted and at least two replicates were injected per cycle as well as experimental replicates of n=3. Experiments were performed at 25°C with a flow rate of 30 µL/min in HBS-EP running buffer (10 mM HEPES pH 7.4, 0.15 M NaCl, 3 mM EDTA, 0.005% v/v surfactant P20). Each concentration of Nb2 was run as follows; 120 sec injection, 900 sec dissociation. Kinetic analysis was performed using the Biacore T200 Evaluation software using a global fitting to a 1:1 binding model.

Crystallisation and structure determination

Crystallisation was performed using the GPVI N72Q variant and untagged Nb2. Both proteins were mixed at 75 μ M and the complex was purified using a Superdex 200 increase 10/300 GL gel filtration column equilibrated in 20 mM Tris pH 7.4, 140 mM NaCl. The complex was concentrated to 5 mg/mL. Crystals were generated in 0.2 M calcium acetate, 0.1M sodium cacodylate pH 6.5, 18% PEG8K and diffraction data was collected at the Diamond Light Source i04 beamline.

The CCP4 software suite was used for structure determination. Molecular replacement was performed in PHASER using 2GI7 and 5TP3 as templates. This was followed by model building in COOT and multiple rounds of refinement in REFMAC. Data collection and refinement statistics are shown in Table 1.

Nuclear factor of activated T-cell (NFAT) reporter assay

The Nuclear factor of activated T-cell (NFAT) reporter assay was used for GPVI-signalling detection, following the protocol documented by Tomlinson *et al.*²⁵. DT-40 cells were transfected with 2 μ g each of full length GPVI, FcR- γ chain and NFAT controlled luciferase reporter construct. Transfected cells were incubated with 100 nM of each nanobody for 15 min followed by stimulation upon the addition of 10 μ g/mL collagen or CRP. All readouts were expressed as a percentage of the signal from collagen alone. GPVI surface expression was confirmed by cell labelling samples with HY101 antibody followed by anti-mouse Alexa Fluor-647 secondary antibody staining and performing flow cytometry. The samples were acquired (FL1 and 4) and analysed using an Accuri C6 flow cytometer (BD Biosciences, USA).

Statistics

Results are shown as mean values \pm standard deviation. ELISA assays were performed with n=3 whereas NFAT assays were performed with n= 5. Student two-tailed *t* test was used and P < 0.05 taken as significant.

Results

Testing of nanobodies on recombinant GPVI

The recombinant GPVI used for immunisation and testing consisted of the extracellular D1 and D2 domains fused with the Fc domain from IgG. Immunisation with GPVI-Fc yielded 54 distinct nanobody sequences. The Fc domain was used to test whether the nanobodies recognise this region. The 54 nanobodies were categorized into 33 distinct binding classes on the basis of their complementary determining region 3 (CDR3) sequence, which is the region that confers ligand specificity²⁶. Nanobodies with CDR3 regions with >80 % homology were considered to be in the same binding class. Nanobodies (1 μ M) from each binding class were tested for their ability to recognise a recombinant GPVI-Fc coated surface (Figure 1a). The degree of nanobody binding varied between classes and could be categorised into strong (>50 %), moderate (>20 %) and weak binders (<20 %). Strong binders included Nb2, 21, 35 and 52. Moderate binders included Nb7, 18, 28 and 54. All other nanobodies were considered to be weak binders.

We used a nuclear factor of activated T-cells (NFAT) reporter assay to investigate GPVI signalling in a transfected cell line (Figure 1b). This assay takes advantage of ITAM signalling through Src and Syk tyrosine kinases which results in NFAT-dependent expression of a luciferase reporter²⁵. Collagen stimulated an 8.3 ± 2.8 fold increase in NFAT activity. Nbs 2, 21 and 35 (100 nM) inhibited the increase

by greater than 80 %, and Nbs 5, 22, 25 and 44 inhibited this by more than 50 %. Several nanobodies, Nbs 6, 24, 28-30 and 49, increased the response to collagen and the remainder either had no effect or resulted in inhibition < 50 %. The marked potency of Nbs 2, 21 and 35 is in line with their high affinity for binding to GPVI (Figure 1a).

Evaluation of Nbs 2, 21 and 35 as blocking agents

The most potent nanobodies, Nb2, 21 and 35, were further tested in their ability to inhibit GPVI function. Firstly, their binding to platelets was tested using flow cytometry. All three nanobodies exhibited similar binding to resting and activated platelets in the presence of PAR1 activating peptide (200 μ M) (Figure 2a) suggesting that they recognise both monomeric and dimeric GPVI. Previously, Jung et al.¹⁴ have reported that thrombin stimulates dimerisation of GPVI. Further studies were performed on these nanobodies to investigate the concentration response relationship in binding to GPVI and for inhibition of platelet aggregation and adhesion under flow. Nbs 2, 21 and 35 inhibited platelet aggregation to collagen (5 μ g/mL and CRP (10 μ g/ml) with IC₅₀ values of 172, 85 and 115 nM for collagen, and 1, 22 and 1 nM for CRP, respectively (Figure 2b). The differential IC₅₀ values is likely to reflect binding of collagen to a second receptor on platelets, integrin α 2 β 1.

In a solid-phase binding assay, all three nanobodies blocked the binding of GPVI-Fc (100 nM) to a collagen surface with IC₅₀ values for Nbs 2, 21 and 35 of 18, 61 and 39 nM, respectively (Figure 2c). The binding affinity of the most potent of the three nanobodies, Nb2, to immobilised GPVI and GPVI-Fc was determined by SPR with a calculated equilibrium dissociation constant (K_D) of 0.7 nM \pm 0.03 nM and 0.58 nM \pm 0.06 nM for GPVI-Fc and GPVI respectively (Figure 2d-e). This binding affinity is approximately 25-fold higher than that of the full-length inhibitory GPVI antibody 9012²⁷. The similar binding affinities to monomeric and dimeric GPVI is consistent with the observation that binding of Nb2 to platelets is not altered upon thrombin stimulation. To assess the effect of the most potent anti-GPVI nanobodies on platelet activation and subsequent thrombus formation a whole blood flow adhesion assay was performed. Blood from healthy donors was preincubated with either PBS or 500 nM Nb2, 21 or 35 for 10 minutes, thrombin inhibited, recalcified and then flown over collagen at a shear rate of 1000/s. Quantitative analysis of the images demonstrated that all three Nbs had no significant effect on platelet adhesion under flow (Figure 3b), but that they inhibited the formation of multilayered aggregates (Figure 3c). The platelets that did adhere also had abrogated PS-exposure relative to untreated controls (Figure 3d). The abolition of aggregation and PS exposure, but not adhesion, is consistent with results in GPVI-deficient patients²³.

Nb2 binds close to the CRP binding epitope and reveals a novel domain-swapped dimeric GPVI structure

We next aimed to solve the crystal structure of the most potent of the Nbs, Nb2, with recombinant GPVI. Crystallisation of dimeric GPVI-Fc was not successful so monomeric GPVI was used. For these studies, the single N-glycosylation site at N72 was mutated to glutamine (GPVI NQ). GPVI NQ was mixed with Nb2 in a 1:1 ratio at a concentration of 75 μ M and purified as a complex by gel filtration (Supplemental Figure 4). The crystal structure of this complex was solved with a resolution of 2.2 \AA . The structure revealed the binding epitope of Nb2 and a novel GPVI dimer conformation (Figure 4). The dimer interface consisted of two domain-swapped D2 domains formed through the extension of the C-C' loop region (labelling in accordance with *Horii et al.*²⁸). This extended loop forms a domain swap hinge that extends outwards and folds with an adjacent D2 (Figure 4b). This is in stark contrast with the back to back D2 dimer reported in previous crystal structures²⁸. Additional novel features within the D2 structure are shown in Figure 4b-c. No observed electron density was found between residues K135-R142, which in previous structures forms the C-terminal end of the C-C' hinge loop and the start of the

C' β -strand. In addition, there is a slight shift within the E β -strand, which in previous structures is made up of residues I147-V150 but is formed by residues S144-I148 in the domain swapped structure. The loop between the E and F β -strands forms a short 3_{10} helix which has not been observed in other D2 structures but is present within D1. These small structural changes are likely the result of the extension of the hinge loop towards the adjacent subunit and subsequent destabilisation of the C' β -strand.

The Nb2 binding site was mapped within D1 adjacent to the CRP binding site. Residues involved in the Nb2-GPVI binding interface are shown in Figure 5a. The primary interaction interface is found towards the top of the CRP binding groove within the D1 C' β -sheet and 3_{10} helix found between β E and F strands. This forms a primary binding pocket and polar contacts between nanobody residues within the CDR3 loop with GPVI residues S45-Y47 found within the D1 C' β -sheet, and S61 found in the short 3_{10} helix. Additional contacts within the primary binding site are made between Nb2 CDR1 residue Y31 and GPVI residue Q48. A secondary interaction pocket is located away from the CRP binding groove made by residues Q1 and Y115 of Nb2 interacting with E21, P56 and A57 of GPVI. A summary of binding residues is presented in Supplemental Table 2. The GPVI binding site lies entirely within the CDR3 loop of Nb2 apart from Q1 and Y31. The Nb2 binding site is adjacent to the CRP binding interface (Figure 5b) with the CDR2 loop extending towards the CRP binding site which would induce steric clashes between both ligands. In addition, the binding of the CDR3 loop to the short C' β -sheet of D1 the top of the CRP binding groove induces a small shift of approximately 1.5 Å which causes a small distortion of the groove (Figure 5b). A Ca^{2+} cation can be found bridging two Nb2 subunits, through interactions with the side chain carboxyl group of E6 and peptide backbone carbonyl of G119, and two water molecules resulting in an octahedral Ca^{2+} ion coordination. In summary, the crystallisation of the GPVI-Nb2 complex has revealed that the Nb2 binding site lies in close proximity to the CRP binding site and induces a small conformational change in D1. The structure also reveals a domain swap between the D2 domains.

Truncating the domain swap hinge region prevents GPVI-signalling but not ligand binding

The domain-swapped structure shows a critical role for the C-C' hinge region which, in the original structure of GPVI, was modelled as an unstructured loop region in one of the two GPVI monomers and was not resolved in the other. In a more recent crystal structure of the GPVI dimer in complex with CRP, this hinge region was removed which means that the domain swap would not have been possible, and the structure of GPVI was the same as the original structure (PDB ID: 5OU7). The position of the hinge region in the nanobody bound structure and original GPVI structure is shown in Figure 6a.

Since the hinge truncated variant of GPVI is still able to bind CRP, as shown in the crystal structure, this provides a mechanism of testing the functional significance of the domain swapped structure. We therefore utilised site directed mutagenesis to truncate the length of hinge region (amino acids G¹²⁹DPAPYKN¹³⁶) and prevent formation of the domain swapped dimer configuration both in a recombinant GPVI construct and in full length GPVI (named Δ C-C'). A solid-phase binding assay showed that GPVI-Fc Δ C-C' bound to both collagen- and CRP-coated surfaces in a concentration dependent manner. Calculated EC50 values for binding to collagen were 294 nM compared with 42 nM for GPVI-Fc and 9 nM compared to 2 nM for GPVI-Fc binding to CRP (Figure 6b i). Nb2 showed an increased potency for displacement of the interaction of GPVI-Fc Δ C-C' to collagen and CRP with an IC50 of 51 and 17 nM respectively, compared with 268 and 132 nM for GPVI-Fc WT (Figure 6b ii), reflecting the lower affinity of collagen and CRP for the mutant. This suggests that the collagen and CRP binding site has undergone a small conformational change that results in reduced ligand binding. Nb2 binding to this mutant was comparable to GPVI-Fc with a K_D of $2.6 \text{ nM} \pm 0.4 \text{ nM}$ as determined by SPR (Supplemental Figure 6). Interestingly collagen and CRP were unable to activate full-length GPVI Δ C-C' construct expressed in a cell line using the NFAT reporter assay (Figure 6c). These results provide evidence that the hinge region may be required for maintaining the conformation of the ligand binding domain and for signalling.

Discussion

In this study we have developed a range of nanobodies to GPVI and characterised these using a variety of assays. These studies show the following: (i) a diverse range of nanobodies with sequence differences in their CDR3 domains bind to GPVI; (ii) the most potent of these, Nb2, 21 and 35, bind with nanomolar affinity and block collagen-induced NFAT activation, platelet aggregation and thrombus formation under flow; (iii) a crystal structure reveals Nb2 binds to a site on GPVI which is adjacent to the CRP binding site; and (iv) Nb2 forms a complex with a novel domain-swapped GPVI dimer. Together, the nanobodies form a library of agents for probing GPVI function in platelets. It should be noted that all nanobodies excluding Nbs 6, 11 and 53, were directly displaced by Nb2 in a competition ELISA (data not shown) which suggests most of the nanobodies may bind close to the Nb2 binding site on D1.

The presence of a domain-swapped GPVI-dimer offers a new scaffold to examine GPVI dimerisation. A critical feature of the domain swap is the extension of the C-C' hinge. The construct used to solve the complex crystal structure with CRP was also missing the C-C' hinged loop region and so a domain swapped dimer could not be formed. The construct used by Horii *et al.* for the original GPVI crystal structure did include the hinge loop but the domain swap was not observed, and the back to back dimer conformation was instead reported. The different conformations between the Horii *et al.* structure and the domain-swapped structure we describe here could be due to the different crystallisation conditions utilised between experiments. A second explanation is that the nanobody stabilises the domain swapped conformation in the crystal and represents just one potential dimeric conformation adopted by GPVI. Dimerisation of recombinant D1,D2 has not been detected in solution²⁸ and the formation of stable dimers likely requires additional contact regions such as the disulphide formed within the intracellular tail²⁹.

By producing a GPVI deletion mutant with a shortened hinge region we have attempted to address the functional significance of the domain-swapped GPVI conformation. In the original non-domain swapped structure (PDB:2GI7), the C-C' loop does not form a domain swap hinge but forms a disordered loop that points away from the rest of the protein (Figure 5b), therefore, shortening this loop would not have a significant impact on GPVI structure unless a domain swap is formed. This is supported by a previously solved structure of GPVI without the C-C' loop (PDB:5OU7) that shows no significant conformational changes within D1 or D2 compared with the original structure. Strikingly, collagen and CRP were unable to activate the hinge mutant which, although not direct evidence for the presence of a domain-swap, does suggest that the domain swap may be important for GPVI signalling. Although binding to CRP and collagen is slightly reduced in the mutant, binding still occurs and the reduction in binding affinity would not result in complete abolition of signalling. However, these results do not definitively prove the existence of a domain-swap. The hinge region may have alternative functions such as being an allosteric modulator of GPVI upon ligand binding. The inability to detect recombinant GPVI dimers in solution is a limiting factor for this study, and other cell line techniques such as nanoBRET³⁰ would need to be performed to confirm the role of the hinge region in GPVI dimerisation.

The crystal structure of Nb2 bound GPVI reveals that Nb2 interacts with the top of the CRP binding groove and, although not directly overlapping with the CRP binding site, is close enough to sterically hinder the binding to collagen. Inhibition of collagen binding by Nb2 is likely however a combination of steric clashes between closely positioned binding sites as well as the distortion of the CRP binding groove, shown in Figure 5c, indicative of a mixed mode allosteric and competitive inhibitor. Nb2 therefore provides a new scaffold that can be used for the development of anti-thrombotic drugs to treat cardiovascular disease.

In summary, our results provide evidence that GPVI signalling requires an active domain swapped conformation of GPVI and offers a new mechanistic insight into GPVI activation. Full-length structures

of GPVI in both resting and activated states are required to confirm the role of the domain-swapped conformation in GPVI activation.

Acknowledgements

This research was funded, in whole or in part, by a Wellcome Trust Investigator Award (204951/B/16/Z). A CC BY licence is applied to the AAM arising from this submission, in accordance with the grant's open access conditions. SPW is a British Heart Foundation Professor (CH 03/003). We acknowledge the Diamond Light Source for provision of synchrotron radiation in using the beamline I04. NJ is supported by the European Union's Horizon 2020 research and innovation program under the Marie Skłodowska-Curie grant agreement No. 766118, and is registered in the PhD programs of Maastricht and University of Birmingham.

Authorship contributions

A. Slater performed experiments, generated new constructs, performed X-ray crystallography, wrote and edited manuscript. Y. Di expressed and performed characterisation experiments on all the nanobodies. J. C. Clark performed flow cytometry experiments. N. Jooss performed flow studies on thrombus formation and edited the manuscript. E. M. Martin performed SPR experiments. F. Alenazy performed platelet aggregation assays. M. Thomas provided supervision and funding. R. Ariens contributed to study design and supervision. A. Herr provided GPVI constructs and training for GPVI production. N. Poulter contributed to study design, provided supervision and edited the manuscript. J. Emsley provided X-ray crystallography supervision, funding and wrote and edited the manuscript. S. P. Watson provided supervision, funding, study design and concept, reviewed data, wrote and edited manuscript. All authors have read the manuscript.

Conflicts of interest disclosure

The authors declare no competing financial interests.

ORCID profiles

A.S., 0000-0001-7166-438X. S.P.W., 0000-0002-7846-7423. M.R.T., 0000-0001-7048-7764, R.A., 0000-0002-6310-5745, A.B.H., 0000-0002-3598-3399. N.S.P., 0000-0002-3187-2130.

References

1. Andrews RK, Arthur JF, Gardiner EE. Targeting GPVI as a novel antithrombotic strategy. *J Blood Med.* 2014;5:59-68.
2. Nieswandt B, Watson SP. Platelet-collagen interaction: is GPVI the central receptor? *Blood.* 2003;102(2):449-461.
3. Mammadova-Bach E, Ollivier V, Loyau S, et al. Platelet glycoprotein VI binds to polymerized fibrin and promotes thrombin generation. *Blood.* 2015;126(5):683-691.
4. Alshehri OM, Hughes CE, Montague S, et al. Fibrin activates GPVI in human and mouse platelets. *Blood.* 2015;126(13):1601-1608.
5. Moroi M, Jung SM. Platelet glycoprotein VI: its structure and function. *Thromb Res.* 2004;114(4):221-233.
6. Zheng YM, Liu C, Chen H, Locke D, Ryan JC, Kahn ML. Expression of the platelet receptor GPVI confers signaling via the Fc receptor gamma -chain in response to the snake venom convulxin but not to collagen. *J Biol Chem.* 2001;276(16):12999-13006.

7. Smethurst PA, Joutsu-Korhonen L, O'Connor MN, et al. Identification of the primary collagen-binding surface on human glycoprotein VI by site-directed mutagenesis and by a blocking phage antibody. *Blood*. 2004;103(3):903-911.
8. Lecut C, Arocas V, Ulrichs H, et al. Identification of residues within human glycoprotein VI involved in the binding to collagen: evidence for the existence of distinct binding sites. *J Biol Chem*. 2004;279(50):52293-52299.
9. Ezumi Y, Shindoh K, Tsuji M, Takayama H. Physical and functional association of the Src family kinases Fyn and Lyn with the collagen receptor glycoprotein VI-Fc receptor gamma chain complex on human platelets. *J Exp Med*. 1998;188(2):267-276.
10. Séverin S, Nash CA, Mori J, et al. Distinct and overlapping functional roles of Src family kinases in mouse platelets. *J Thromb Haemost*. 2012;10(8):1631-1645.
11. Suzuki-Inoue K, Tulasne D, Shen Y, et al. Association of Fyn and Lyn with the proline-rich domain of glycoprotein VI regulates intracellular signaling. *J Biol Chem*. 2002;277(24):21561-21566.
12. Watson SP, Auger JM, McCarty OJ, Pearce AC. GPVI and integrin alphaIIb beta3 signaling in platelets. *J Thromb Haemost*. 2005;3(8):1752-1762.
13. Jung SM, Tsuji K, Moroi M. Glycoprotein (GP) VI dimer as a major collagen-binding site of native platelets: direct evidence obtained with dimeric GPVI-specific Fabs. *J Thromb Haemost*. 2009;7(8):1347-1355.
14. Jung SM, Moroi M, Soejima K, et al. Constitutive dimerization of glycoprotein VI (GPVI) in resting platelets is essential for binding to collagen and activation in flowing blood. *J Biol Chem*. 2012;287(35):30000-30013.
15. Loyau S, Dumont B, Ollivier V, et al. Platelet glycoprotein VI dimerization, an active process inducing receptor competence, is an indicator of platelet reactivity. *Arterioscler Thromb Vasc Biol*. 2012;32(3):778-785.
16. Miura Y, Takahashi T, Jung SM, Moroi M. Analysis of the interaction of platelet collagen receptor glycoprotein VI (GPVI) with collagen. A dimeric form of GPVI, but not the monomeric form, shows affinity to fibrous collagen. *J Biol Chem*. 2002;277(48):46197-46204.
17. Poulter NS, Pollitt AY, Owen DM, et al. Clustering of glycoprotein VI (GPVI) dimers upon adhesion to collagen as a mechanism to regulate GPVI signaling in platelets. *J Thromb Haemost*. 2017;15(3):549-564.
18. Hassanzadeh-Ghassabeh G, Devoogdt N, De Pauw P, Vincke C, Muyltermans S. Nanobodies and their potential applications. *Nanomedicine (Lond)*. 2013;8(6):1013-1026.
19. Hamers-Casterman C, Atarhouch T, Muyltermans S, et al. Naturally occurring antibodies devoid of light chains. *Nature*. 1993;363(6428):446-448.
20. Onselaer MB, Hardy AT, Wilson C, et al. Fibrin and D-dimer bind to monomeric GPVI. *Blood Adv*. 2017;1(19):1495-1504.
21. Raynal N, Hamaia SW, Siljander PR, et al. Use of synthetic peptides to locate novel integrin alpha2beta1-binding motifs in human collagen III. *J Biol Chem*. 2006;281(7):3821-3831.
22. Ungerer M, Rosport K, Bültmann A, et al. Novel antiplatelet drug revacept (Dimeric Glycoprotein VI-Fc) specifically and efficiently inhibited collagen-induced platelet aggregation without affecting general hemostasis in humans. *Circulation*. 2011;123(17):1891-1899.
23. Nagy M, Perrella G, Dalby A, et al. Flow studies on human GPVI-deficient blood under coagulating and noncoagulating conditions. *Blood Adv*. 2020;4(13):2953-2961.
24. van Geffen JP, Brouns SLN, Batista J, et al. High-throughput elucidation of thrombus formation reveals sources of platelet function variability. *Haematologica*. 2019;104(6):1256-1267.
25. Tomlinson MG, Calaminus SD, Berlanga O, et al. Collagen promotes sustained glycoprotein VI signaling in platelets and cell lines. *J Thromb Haemost*. 2007;5(11):2274-2283.
26. Bannas P, Hambach J, Koch-Nolte F. Nanobodies and Nanobody-Based Human Heavy Chain Antibodies As Antitumor Therapeutics. *Front Immunol*. 2017;8:1603.

27. Lebozec K, Jandrot-Perrus M, Avenard G, Favre-Bulle O, Billiald P. Design, development and characterization of ACT017, a humanized Fab that blocks platelet's glycoprotein VI function without causing bleeding risks. *MAbs*. 2017;9(6):945-958.
28. Horii K, Kahn ML, Herr AB. Structural basis for platelet collagen responses by the immune-type receptor glycoprotein VI. *Blood*. 2006;108(3):936-942.
29. Arthur JF, Shen Y, Kahn ML, Berndt MC, Andrews RK, Gardiner EE. Ligand binding rapidly induces disulfide-dependent dimerization of glycoprotein VI on the platelet plasma membrane. *J Biol Chem*. 2007;282(42):30434-30441.
30. Machleidt T, Woodrooffe CC, Schwinn MK, et al. NanoBRET--A Novel BRET Platform for the Analysis of Protein-Protein Interactions. *ACS Chem Biol*. 2015;10(8):1797-1804.

Data collection	Value
Space group	P 21 21 21
Cell dimensions	
a, b, c (Å)	69.91 84.75 124.04
α, β, γ (°)	90.00 90.00 90.00
Resolution (Å)	84.57– 2.5
R merge	0.122 (0.595)*
I/ σ I	8.67 (2.69)*
Completeness (%)	100 (98.6)*
Redundancy	6.3 (6.4)*
Wavelength	0.96864 Å
Refinement	
No of reflections	26173
R _{work} ^b / R _{free} (%)	0.176 / 0.232
No. atoms	
Protein	4664
Ca ²⁺	1
Water	271
B-factors (Å²)	
Protein	43.91
Metal	24.33
Water	41.78
R.m.s deviations	
Bond lengths (Å)	0.0084
Bond angles (°)	1.568

Table 1: Crystallographic data collection and refinement statistics.

*Values in parentheses are for highest-resolution shell.

$aR_{merge} = \sum_h \sum_i | \langle I_h \rangle - I_{h,i} | / \sum_h \sum_i I_{h,i}$ where I is the observed intensity and $\langle I_h \rangle$ is the average intensity of multiple observations from symmetry-related reflections calculated.

$bR_{work} = \sum(h) ||F_o| - |F_c|| / \sum(h)|F_o|$, where F_o and F_c are the observed and calculated structure factors, respectively. R_{free} computed as in R_{work} , but only for (5%) randomly selected reflections, which were omitted in refinement, calculated using REFMAC.

Figure 1. Testing of nanobody binding and inhibition of GPVI signalling. a) Surface binding assay of one nanobody (100 nM) from each binding class to a GPVI-Fc coated-surface. All the binding results have been normalised to Nb35 which gave the highest readout. Binding of each nanobody to the Fc domain-coated surface was tested and subtracted from the GPVI-Fc readings. Binding was detected using HRP conjugated anti-His antibody. The average binding of all the nanobodies to BSA represents a non-specific binding control. Data represent mean values of three experiments \pm standard deviation. b) NFAT reporter assay of GPVI and FcR γ transfected DT40 cells stimulated by collagen (10 μ g/ml) in the presence of the nanobodies (100 nM). Results were plotted as a percentage of total signalling in the presence of collagen only. Dotted lines represent 100, 50 and 20 % signalling levels and nb2, 21 and 35 are coloured in black, red and orange respectively. Data represent mean values of three experiments performed in triplicate \pm standard deviation.

Figure 2. Further testing of top inhibitory nanobodies of GPVI. a) Nanobodies 2, 21 and 35 (5 μ M) binding to washed platelets in the presence or absence of 200 μ M PAR1 by flow cytometry. Grey histograms show unstained washed platelets, black histograms show non-specific staining of anti-his alexafluor647 secondary, red histograms show nanobody binding to resting platelets and green histograms show nanobody binding to PAR1 peptide-activated platelets. b) Platelet aggregation in response to i) 5 μ g/mL collagen and ii) 10 μ g/mL CRP in the presence of Nb2, 21 and 35. Top panel shows representative aggregation curves for Nb2 whereas the bottom panel shows max aggregation values for all nanobodies. IC₅₀ values of 172, 85 and 115 nM for collagen and 1, 22 and 1 nM for CRP were determined for Nb2, 21 and 35, respectively. The effect of different concentrations of the nanobody compared to the vehicle (PBS) was determined using two-way ANOVA with Dunnett's correction for multiple comparisons. c) Solid-phase binding assay showing GPVI-Fc (100 nM) displacement from a collagen surface in the presence of increasing concentration Nb2, 21 and 35, with IC₅₀ values of 18, 62 and 39 nM respectively. Data represent mean values of three \pm standard deviation. d-e) SPR data showing Nb2 at a range of concentrations binding to GPVI-Fc (d) and GPVI (e) immobilised on a surface. The binding affinity was determined by kinetic analysis with calculated K_D values of 0.7 nM \pm 0.03 nM for GPVI-Fc and 0.58 nM \pm 0.06 nM for GPVI.

Figure 3. Effect of anti-GPVI nanobodies in whole blood microfluidics. a) Representative images of whole blood perfused at an arterial shear rate (1000/s) over Horm Collagen I in the presence of either PBS, 500 nM nanobody 2, 21 or 35. Adhered platelets and platelet aggregates were imaged in brightfield after 3.5 minutes of flow. Platelets were labeled with Annexin V AF568 to assess phosphatidylserine (PS) exposure. All images were taken on an EVOS AMF4300 using a 60x, 1.42NA oil objective. Data are representative of 2 runs for each of 3 donors per treatment. Scale bar: 50 μ m. Quantitative analysis of the images assessed the effect of the nanobodies on percentage of total surface area covered by b) platelets, c) multilayered thrombi and d) platelets exposing PS. Data points are individual runs for each of 3 donors (shown in different colours) per treatment (Mean \pm SD). Unpaired t-test with Mann Whitney correction was employed to test for statistical significance, ** $p < 0.005$. SAC = Surface area coverage.

Figure 4. Crystallisation of Nb2 and GPVI. a) Structure of Nb2 binding to GPVI. (i) A side view of the GPVI-Nb2 structure; (ii) A top down view illustrating the domain swap hinge region. A cartoon representation is shown below each figure. Separate GPVI protein subunits are shown in green and cyan, and both Nb2 proteins are shown in yellow and pink. The domain-swapped D2 domains are labelled D2a and D2b for the N and C-terminal D2 regions respectively. b) Comparison of the D2 domains from the non-domain swapped structure (PDB: 2GI7) (bi) and the domain swapped structure (bii) with major features highlighted. This highlights the differences within the C-C' hinge region, the C' β -strand where no electron density was observed for the domain swapped structure and the presence of an 3_{10} helix between β E and F. c) Zoomed in view of the D2 domain swap hinge region with the hinge loops coloured in green and cyan and the inter-chain polar contacts, which stabilise this region, shown as red dashes.

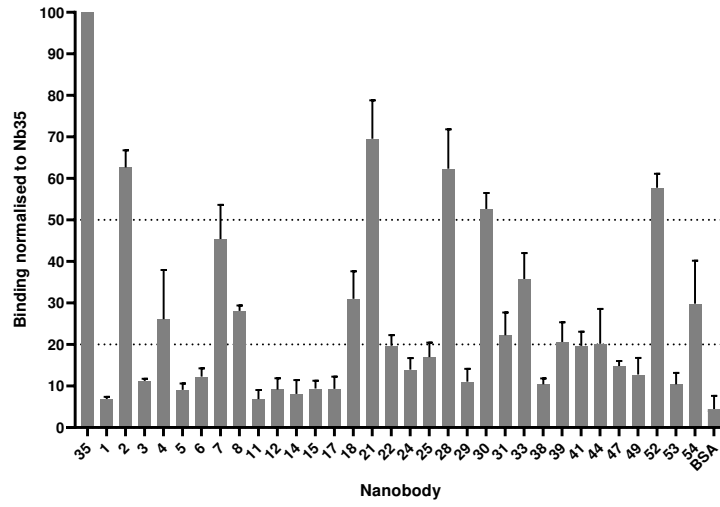
Figure 5. Site of interaction of GPVI with Nb2 and CRP. a) Zoomed in view of the GPVI : Nb2 binding interface. GPVI is coloured in light green, and Nb2 binding residues in the CDR3 loop are coloured in blue and non-CDR3 residues in pink. Red dashed lines indicate polar contacts made between GPVI and Nb2 residues. The full CDR3 sequence for Nb2 is provided underneath the structure with binding residues highlighted in bold. b) Zoomed in view of the CRP binding groove of the CRP bound GPVI structure (pink) and nanobody bound structure (green), with CRP shown in cyan and Nb2 cdr3 residues 100-105 shown in blue. The binding of Nb2 towards the top of the binding groove results in a shift of the β C' sheet resulting in a small distortion of the CRP binding groove. c) Locations of the known Nb2 and CRP binding sites on GPVI. i) Surface representation of Nb2 (pink) modelled onto the GPVI-CRP complex structure (PDB: 5OU8), coloured in green and cyan respectively, revealing the two non-overlapping but closely situated binding sites. ii) Nb2 and CRP binding residues mapped as pink and cyan spheres respectively on the structure of GPVI.

Figure 6. The domain swap is required for signalling but not ligand binding. Ai and ii) Crystal structures of the nanobody bound and original unbound GPVI structures respectively, highlighting the region of the C-C' hinge loop (coloured in orange) deleted for mutation studies. The domain swapped structure contains two GPVI subunits coloured in green and cyan whereas only one subunit is shown for the original GPVI structure. The domain-swapped D2 domain is labelled D2a and D2b for the N

and C-terminal D2 regions respectively. bi) Solid-phase binding assay comparing the dose-dependent binding of GPVI-Fc and GPVI-Fc Δ C-C' to collagen and CRP coated surface. Respective EC50 values of 42 and 294 nM were calculated for GPVI and GPVI Δ C-C' binding to collagen and 2 and 9 nM for CRP. ii) The binding of GPVI-Fc and GPVI-Fc Δ C-C' to a collagen and CRP-coated surface and subsequent displacement by increased concentrations of Nb2. 500 nM GPVI was used for collagen and 100 nM GPVI was used for CRP. Data has been normalised against the highest and lowest concentrations of Nb2 and is expressed as % binding. Respective IC50 values of 268 and 51 nM were calculated for GPVI and GPVI Δ C-C' binding to collagen and 132 and 17 nM for CRP. Data represent mean values of three experiments \pm standard deviation. c) NFAT-reporter assay of DT40 cells transfected with the FcR- γ chain and either full length GPVI WT or hinge mutant. Luciferase activity was reported for non-stimulated, CRP and collagen stimulated cells. Data represent mean values of five experiments performed in triplicate \pm standard deviation and values are normalised against the respective basal levels. A student two-tailed *t* test was used to determine significance between basal and stimulated values.

Figure 1

a)



b)

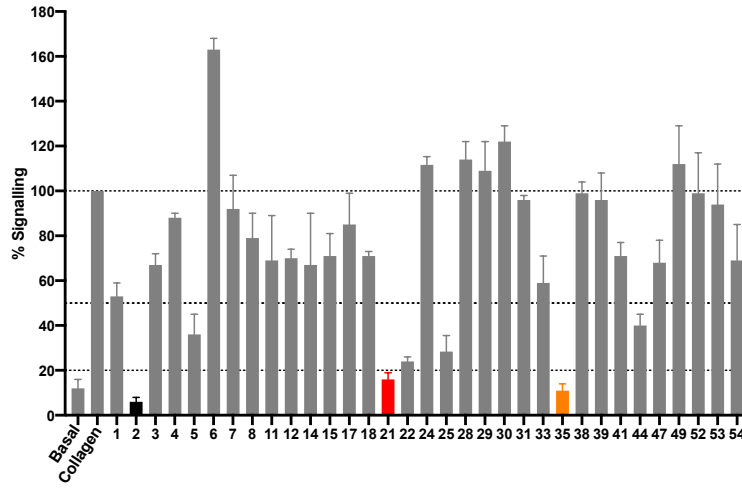
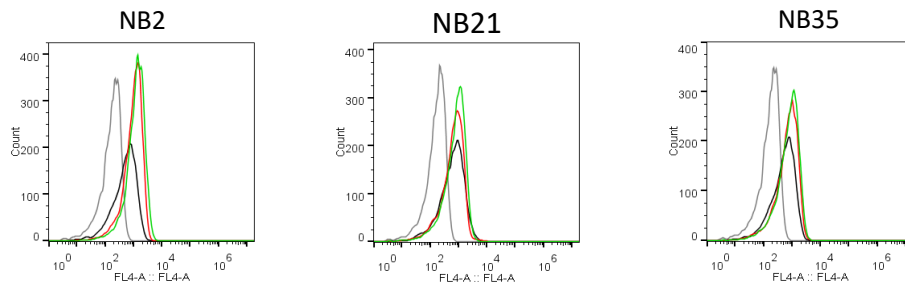
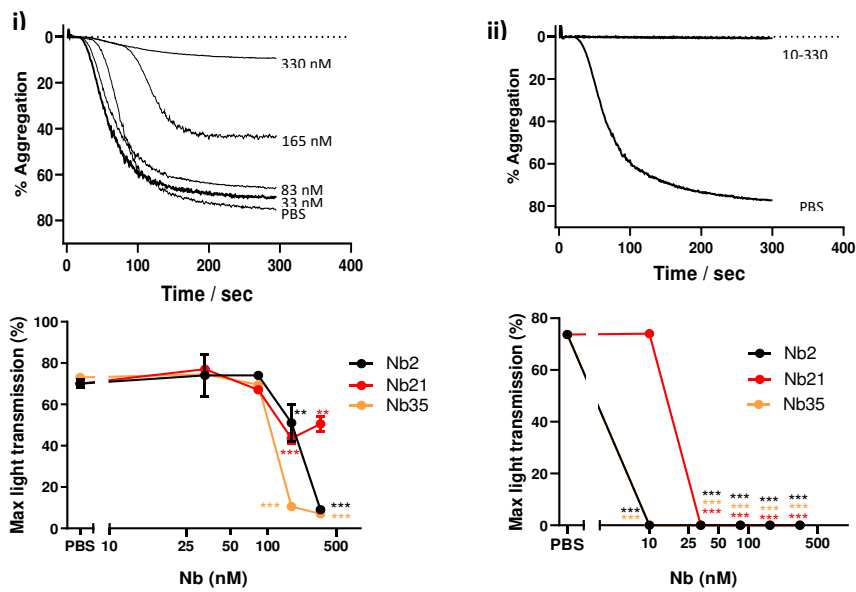


Figure 2

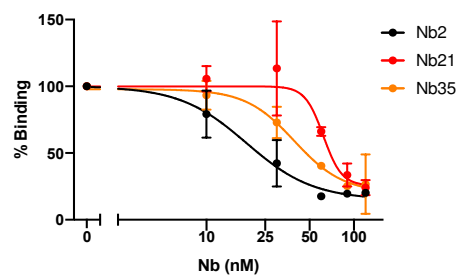
a)



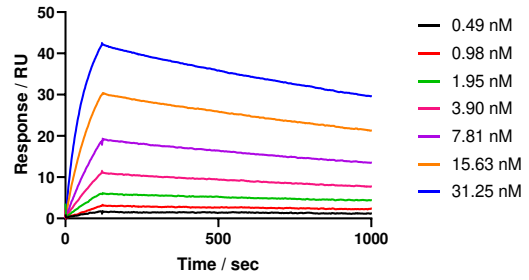
b)



c)



d)



e)

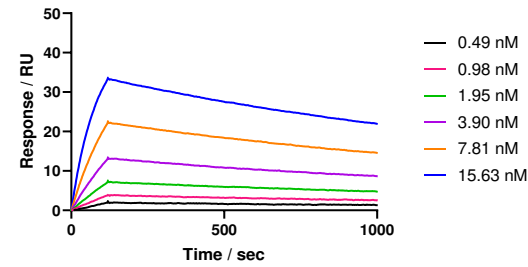


Figure 3

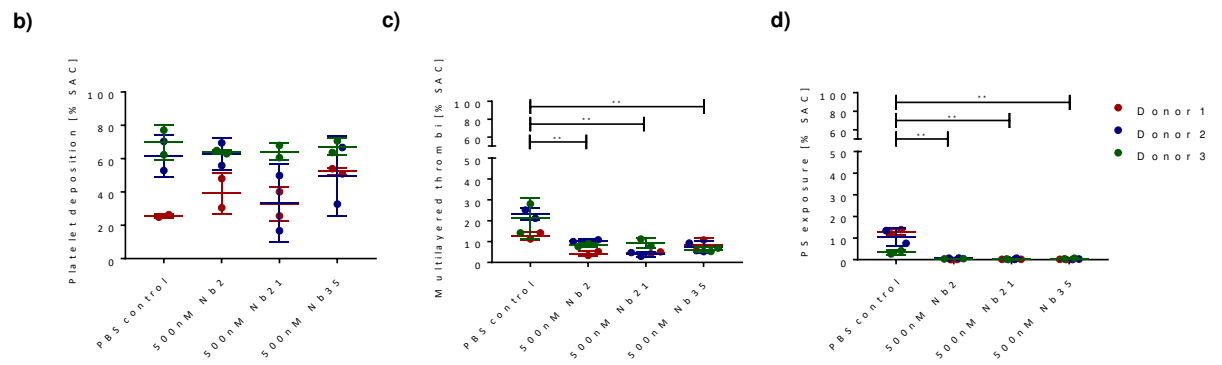
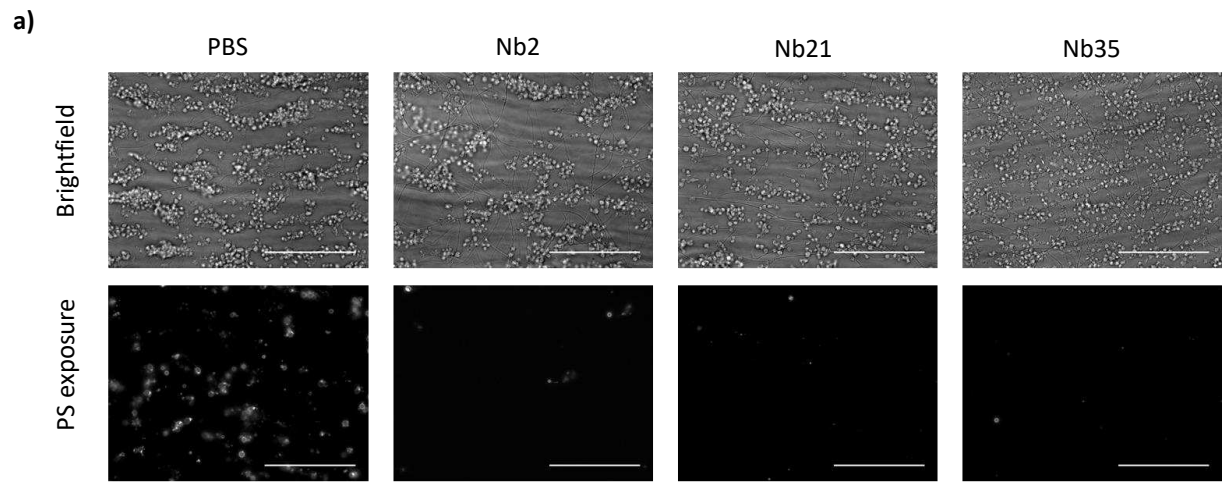


Figure 4

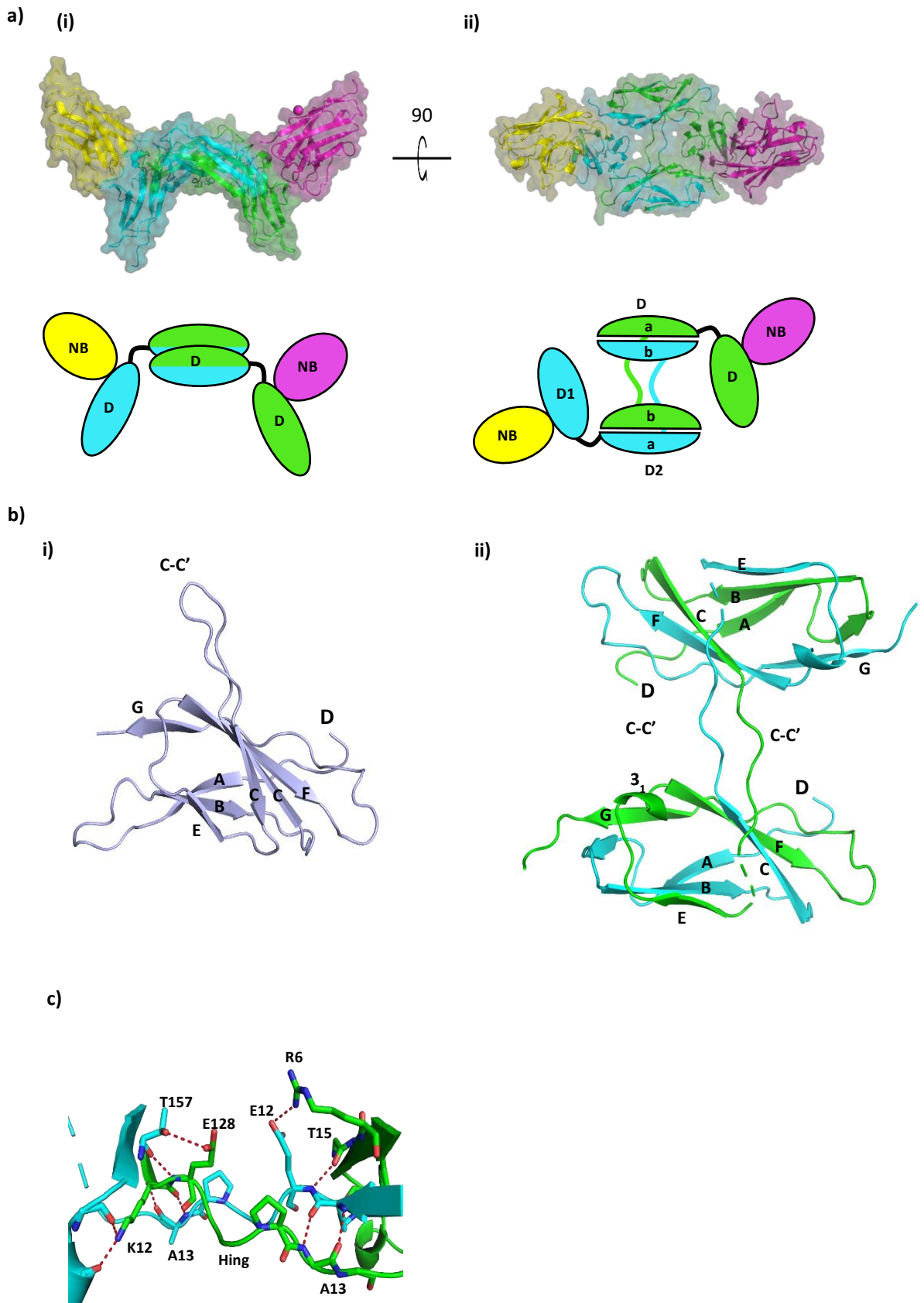


Figure 5

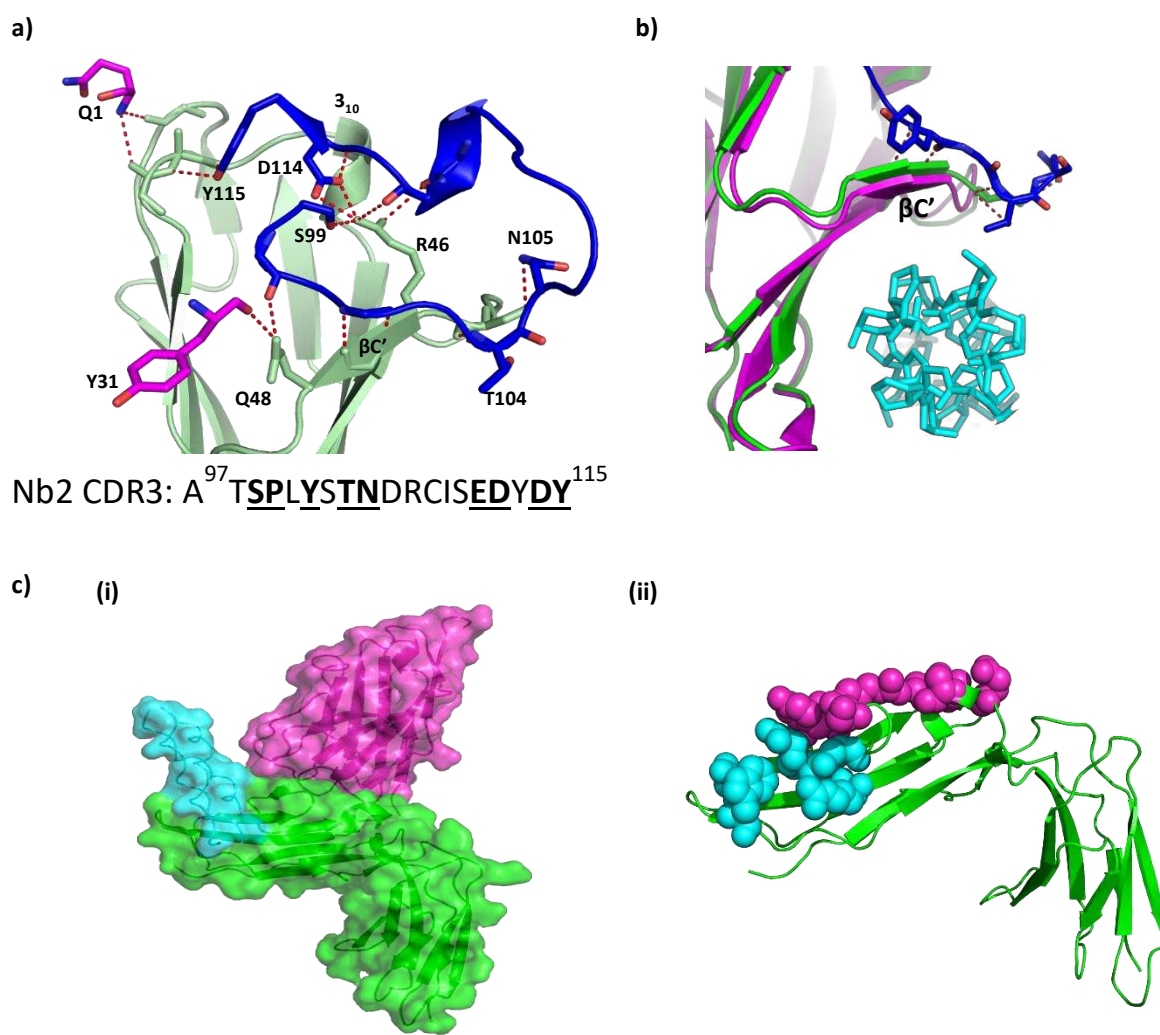
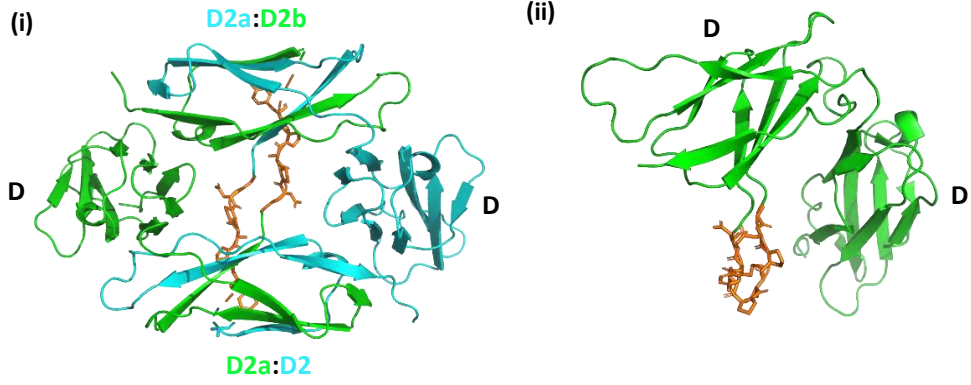
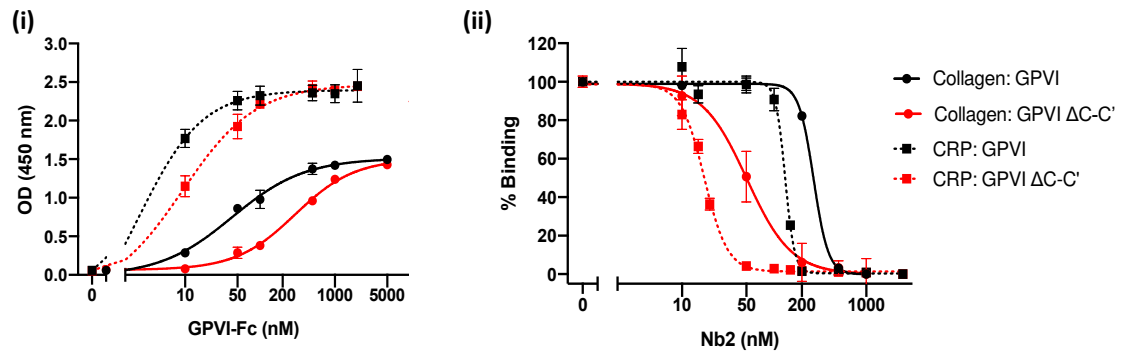


Figure 6

a)



b)



c)

